

# Development of an Inexpensive Tri-axial Force Sensor for Minimally Invasive Surgery

Lu Li<sup>1</sup>, Bocheng Yu<sup>1</sup>, Chen Yang<sup>1</sup>, Prasad Vagdargi<sup>1</sup>, Rangaprasad Arun Srivatsan<sup>1</sup> and Howie Choset<sup>1</sup>

**Abstract**—This work presents the design and evaluation of a low-cost tri-axial force sensor, that has been developed to regain the sense of touch in minimally invasive surgeries (MIS). The force sensor uses an array of force sensitive resistors (FSR) with a mechanically pre-loaded structure to perform the force sensing. The sensor has a built-in signal conditioning circuitry to provide on-board power regulation, programmable signal amplification and analog to digital conversion. The sensor is inexpensive and highly sensitive to low-amplitude force, critical in surgical applications. We validate the efficacy of the sensor with two surgical applications - robotic palpation for stiffness mapping and obstacle avoidance for a highly articulated robotic probe (HARP). The results show that the sensor is capable of accurately detecting the stiff inclusions embedded in the tissues as well as detecting obstacles and helping HARP safely navigate around them.

## SUPPLEMENTARY MATERIAL

This paper is accompanied by a video:  
<https://youtu.be/gmXQZuhdCLA>

## I. INTRODUCTION

Minimally invasive surgery (MIS) has become a preferred means of surgery over the past few decades. The main advantages of MIS over open surgery are reduced trauma, risks of infection and duration of hospital stay. More recently, robot assisted MIS has gained popularity due to the increased precision and dexterity offered by robots. Surgical robots such as the da Vinci surgical system [1], surgical snake robots [2] and continuum manipulators [3] provide increased dexterity to the surgeon and facilitate effective minimally invasive surgeries. These robots are typically teleoperated using visual feedback from stereo vision systems. Lack of tactile or force feedback in such systems results in the over dependence on visual information, leading to increased tissue trauma and damage [4]. This work introduces a design for an inexpensive miniature tri-axial force sensor which can be used in MIS.

Our design incorporates a force sensitive resistor (FSR) array, an innovative mechanical structure and a custom designed onboard electronics in a cost-effective package as shown in Fig. 1. The sensor design is unique compared to traditional FSR-based force sensors [5] in its ability to perceive low-amplitude force (less than 1 N) with built-in signal processing, combined with the ability to decode multi-axis force vector in a low-profile package. Another important aspect of our design is the low-cost and ease of fabrication.

<sup>1</sup>The authors are with the Biorobotics Lab, Robotics Institute, Carnegie Mellon University, Pittsburgh, PA 15213, USA (luli1988@, bochengy@andrew, chenyan1@andrew, prasadv@, rarunsrivatsan@, choset@cs.) cmu.edu

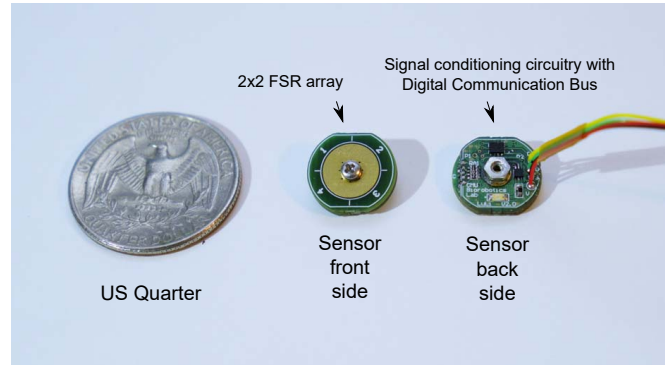


Fig. 1: Force sensor assembly.

The technical specification of the sensor can be found in Table I.

To evaluate the performance of the sensor under surgical scenarios, we conducted two experiments – force controlled palpation for detection of stiff inclusions and obstacle avoidance for a highly articulated robotic probe (HARP).

TABLE I: Technical specification of the force sensor.

Dimensions	$\phi 12\text{mm} \times 3\text{mm}$
Mass	1g
Voltage	DC 3.5V to 5.5V
Current	15mA@5.0V
Communication	Inter-Integrated Circuit (I2C) bus
Sample Rate	up to 860 samples per second (SPS)
Amplifier Gain Factor	2/3, 1, 2, 4, 8, or 16
Sensing Range	0 – 8 N (Gain factor = 1)
Minimal Force Resolution	0.1 N (Gain factor = 1)
Angular Decoding Accuracy	$\pm 10$ Degree
Optimal Working Temperature	50 to 120°F (10 to 50°C)
Hardware Cost	\$10 (mid-volume manufacturing)

## II. BACKGROUND

Lack of force feedback makes it difficult for the surgeons to perform several tasks in MIS such as palpation, tissue retraction and tumor detection [4]. Advances in robotics, haptics, fabrication techniques and computer-integrated surgery have the potential to significantly improve MIS by developing force and tactile sensing modalities and providing feedback to regain the lost sense of touch [6], [7], [8].

Several approaches have been developed for force sensing, the most common one being the use of displacement

sensors such as potentiometers, linear variable differential transformers (LVDT) and Hall-effect sensors [9]; and related the measured displacement to the force. However, errors in displacement measurements resulting from joint friction and backlash in mechanical drive can adversely affect the force [6].

Strain gauges are another popular option used for force sensing. Baki *et al* [10] developed a tri-axial miniature force sensor using strain gauges. Strain gauges have also been used for intrinsic force sensing in continuum robots [11]. In general, complicated fabrication procedures and low sensitivity are the major limitations of strain gauge-based sensors.

When compared with the strain gauges, capacitance-based sensors can achieve higher sensitivity in force measurements [12]. Gray and Fearing [13] designed a miniature  $8 \times 8$  tactile capacitive array sensor that has a size smaller than  $1\text{mm}^2$  and is able to measure force accurately with mN precision. Even though capacitance-based sensors suffer from severe hysteresis problems and a relatively small range of force sensing, they remain attractive for developing miniature MIS devices [14].

Piezoelectrics are very unique means of force sensing, due to their ability to generate large voltages when subjected to even small deformations hence do not need an external power supply [15]. Dargahi *et al.* [16] used polyvinylidene fluoride polymer to develop a miniature tactile sensor that shows very high sensitivity, good linearity and high signal-to-noise ratio. Other researchers have developed similar sensors with different form factors [17], [15]. The main drawback of piezoelectrics is sensitivity to temperature and the instability due to charge leakages when measuring static forces.

In contrast with the piezoelectric sensors, the FSR sensor is a slow device with a mechanical rise time of 1-2ms and is usually less sensitive to small vibrations and low amplitude [18]. In addition a key issue with FSR sensors is the tendency to drift in resistance under constant load. However, FSR sensors are more shock resistant, robust and can work in temperature ranges of room temperature to  $170^\circ\text{C}$  and is relatively insensitive to humidity [18]. The design of the FSR sensor presented in our work handles the above mentioned drawbacks while benefitting from the inherent robustness of the sensor material and the flexibility of designing arbitrary sensor shape or even hollow structure.

Optics-based force sensors have been reviewed by Puangmali *et al.* [6]. These sensors offer several benefits such as small size, high sensitivity, accuracy and MRI compatibility. The only drawback is the complexity involved in the fabrication of these sensors, because of the presence of several small and intricate parts to be fabricated and assembled alongside miniature circuitry.

When using robot manipulators for force sensing, the current in the actuated joints can be used to measure the applied force. This sensing modality is different from the others in that it can measure the force and torque applied over the entire length of the robot and not just the end-effector. The forces at the actuated joints are usually proportional to the current in the motors. But the accuracy of the measured

force is compromised due to several effects of friction in the joints, backlash due to gear-box, changes of the motor brush conductivity and winding resistance [19]. Tadano *et al.* [20] showed with their pneumatic 4-DOF forceps that if pneumatic actuators are used, forces can be estimated with a reasonably good sensitivity and accuracy.

### III. SENSOR DESIGN

#### A. Design Requirements

Three requirements dominate the sensor design choices:

- 1) The physical dimensions of the sensor need to be small and low-profile, so that it can be attached to a robot end-effector or tool used in MIS.
- 2) Surgical applications such as palpation require a highly sensitive sensor, that responds to small amplitude force perception and has a basic comprehension of multi-axis force vector decoding.
- 3) The sensor needs to be inexpensive compared to existing miniature force sensing solutions so that it will be more affordable and accessible to people in need.

In addition, it is also desirable to design all the components of the sensor by following a modular and reconfigurable approach. This would allow any element of the sensor to be replaced or swapped for an upgrade or maintenance. While we present a specific design in this paper, our approach enables the user to modify the hardware as demanded by the application. For example, the electrode boards can be redesigned to have a different diameter and/or a different array density from the one presented in this paper, without changing the design of the other components and the software to reduce development risk and cost.

#### B. Theory of Operation

Our design contains four electrodes with a thin sheet polymer consisting of both electrically conducting and non-conducting particles embedded within it [5]. A force applied to the polymeric film brings the particles in contact with the electrode plate and reduces the resistance of the film.

For this application, various polymeric films, from Tekscan, Creativematerials and Adafruit, were evaluated and the 3M Velostat film was selected for its repeatability in sensing. This material is also inexpensive and available in a variety of sheet thickness for use in various applications [21], [22]. FSRs are generally classified according to their two modes of construction. Both of them are two terminal, multilayer devices, but exhibit different force-resistance behaviors [23].

- 1) **Shunt mode:** Shunt mode is the commonly used method of construction which consists of a solid area of semiconductive polymer on a flexible substrate, as shown in Fig. 2(a). The bottom layer further consists of traces of conductive material arranged as two sets of interdigitating fingers. Exerting force on the material shunts the two traces and varies the resistance.
- 2) **Thru mode:** Thru mode construction uses a semiconductive polymer deposited on an electrode completely

covering the conductor. The polymer is layered between the electrodes, as shown in Fig. 2(b). Thru mode FSR responds faster and behave linearly during force loading phase. Besides, thru mode FSRs can be force preloaded, which reduces the minimum force required for contact detection and results in a decrease in the nonlinearity of the measurements.

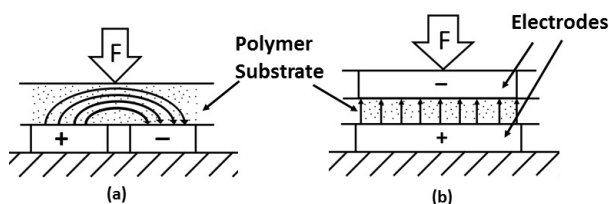


Fig. 2: Two operating modes of the FSR (a) Shunt mode and (b) Thru mode.

The force vector can be estimated from the sensing array using a simplified seesaw model of the forces measured on the tactile array, as illustrated in Fig. 3. A centered fulcrum allows the top layer of electrode to tilt and descend, causing the forces to be transmitted to the polymer substrate layer, resulting changes of its resistance. A non axial force can hence be decoupled into four sensing outputs of the FSR. In this design, we apply this model to a 2D seesaw structure, with the fulcrum placed in the center of a  $2 \times 2$  sensing array and modeled as a combination of a ball joint and prismatic joint. The four sensing elements in this array act as independent variable resistors, whose resistance changes when an external force is applied and provides the magnitude and direction of the contact force.

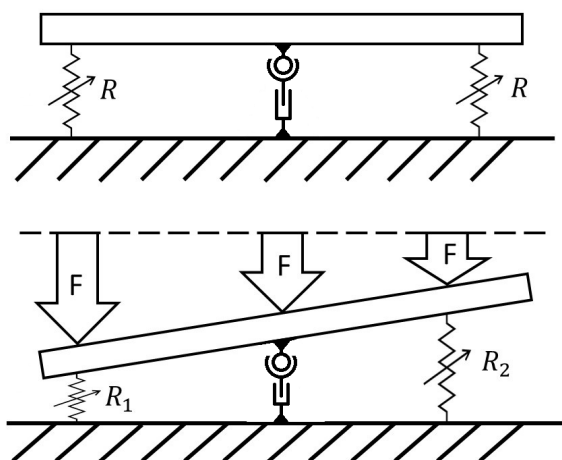


Fig. 3: A simplified seesaw model of the FSR array.

### C. Mechanical Design

The mechanical structure of the force sensor consists of four board layers stacked together as a sandwich structure, as illustrated in Fig. 4. From sensor tip to base, the order is: a common reference electrode board, FSR material, a two

by two array of electrodes board and a signal conditioning board, which are mechanically and electrically connected through a group of size #0-80 fasteners. Optional components such as a protective tip and external fixture can be included to adapt various use-cases.

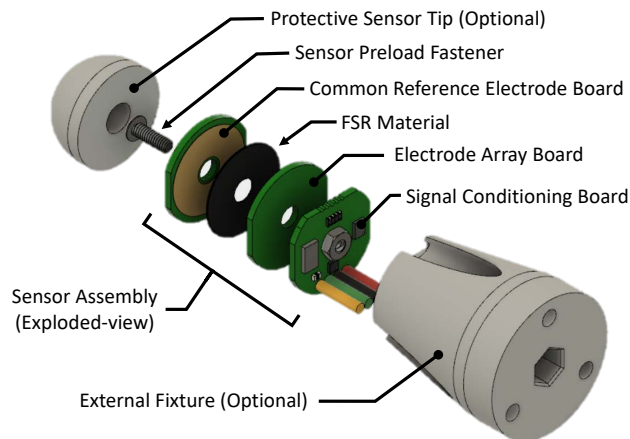


Fig. 4: Exploded view of the force sensor.

The purpose of the #0-80 screw, washer, and nut group is to provide pretension to the board sandwich stacks so that the FSR is always in a preloaded state (see Fig. 5). Due to the fact that a polymer based FSR with thru-mode configuration can detect even a slight amount of force input, our sensor is capable of sensing contact force magnitude in the range of 0 to 10 Newton, with a resolution of 0.1 Newton (Gain factor = 1).

Furthermore, the center aligned fastener allows the common reference electrode board to pivot around the center point like a 2 degree of freedom (DOF) seesaw. In a real world scenario, any contacting force aligned at an angle to the sensor central axis would result in a measurement difference between the arrayed electrodes underneath the FSR materials. The difference in the magnitude of FSR array output is related to the angle and magnitude of the force vectors, and the relationship between these two factors can be obtained by physical modeling or sensor profiling experiments as shown in Sec. VI-A. Thus, this sensor design opens up the potential for decoding 3-DOF force vector by the analysis of multichannel FSR array signals.

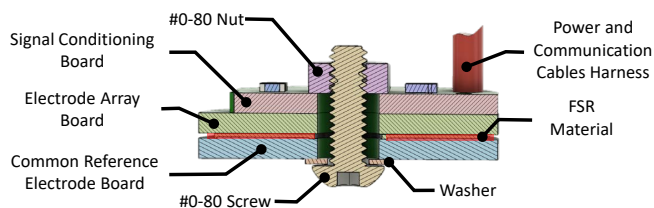


Fig. 5: Cross section view of the sensor.

## IV. ELECTRICAL DESIGN

The on-board electronics design of the force sensor is aimed towards creating a miniature, modular, and inexpensive hardware solution, while enabling maximized performance and reconfigurability. To this end, we leverage the advances in Integrated Circuit (IC) and wearable electronics to further increase sensing performance, reduce footprint dimensions and manufacturing cost. We have developed an innovative approach of custom designing the three major functional blocks of the sensor - the power supply, signal conditioning, and communication circuits.

The schematic drawing of this sensor circuit is illustrated in Fig. 6, and Altium Designer (Altium Limited, Sydney, Australia) software was used to design this sensor.

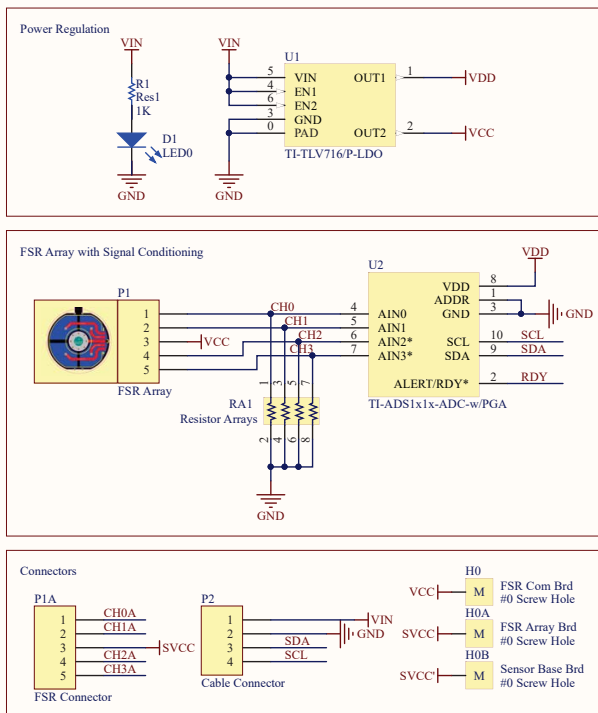


Fig. 6: Schematic drawing of the electrical design.

### A. Power Supply Circuit

The force sensor features a sub-miniature on-board power regulator, the TLV716/P (Texas Instruments Inc., Dallas, Texas, USA), a capacitor-free dual 150mA output voltage regulator in 1.2mm × 1.2mm SON package, which is ideal for dimension and performance sensitive electronics design. This power supply system addresses two major challenges when designing a miniature mixed-signal systems. The specially designed IC eliminates the input and output bypass capacitors which are required in a traditional regulator circuit layout to reduce the surface area and component number counts. The built-in dual power output enables the separation between analog and digital circuits, to further minimize the interference across both the systems. This allows the signal

conditioning circuit to acquire analog signals more accurately and reliably [24].

### B. Signal Conditioning Circuit

The signal conditioning circuit consists of an array of pull-down resistors and an analog to digital converter (ADC). The purpose of this circuitry is to transform the variable resistance of FSR to voltage analog outputs, amplify the signal, convert it to digital data, and eventually transmit the data to a host system through a communication bus.

In this design, we select the ADS1115 ADC (Texas Instruments Inc., Dallas, Texas, USA) for its ultra-small form factor (1.50 mm × 2.00 mm).

### C. Communication Interfaces

The digital communication of the force sensor uses Inter-Integrated Circuit (I2C) as the standard protocol and interface. An external host processor, such as a microcontroller or a PC is necessary to send commands and acquire data from the force sensor via the I2C bus. A ground shielded cable is required if used in an electromagnetic interference sensitive environment. In this setup, an external host processor can connect up to four sensor nodes as its slave devices. Compared to the analog signal bus that is used in traditional FSR sensors, the digital communication bus eliminates the possibility of introducing electromagnetic noise to the analog data along the cable routing path.

## V. FABRICATION AND ASSEMBLY

A 2-layer panelized printed circuit board (PCB) design was manufactured and assembled in small quantity for evaluation. A finished PCB with components is shown in Fig. 7. Three functioning board modules are laid out in one panel, and all surface mount components are located on the same side of the board. Paired with the FSR film and the center fasteners, the final sensor hardware can be quickly assembled and calibrated, as shown in Fig. 1. The strategy of relying on PCB as the main building block of the sensor simplifies the fabrication and assembling process, thus enabling quick production at a minimal cost.

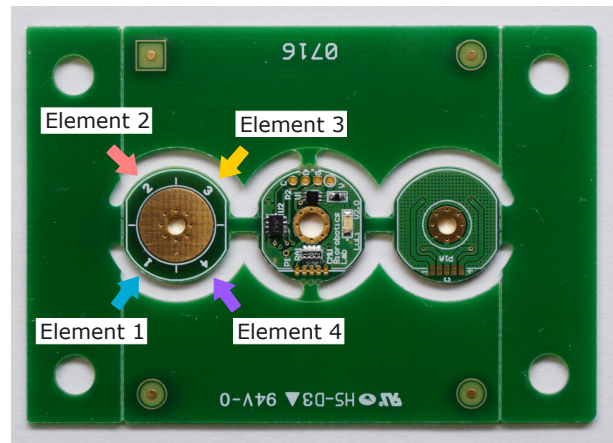
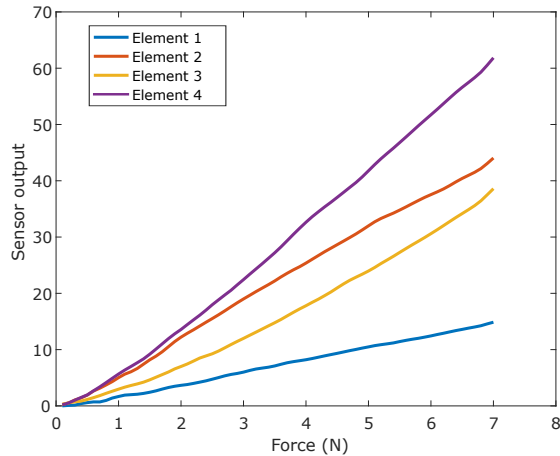


Fig. 7: Panelized PCB after assembly, with the illustration of the position of 4 FSR array elements.

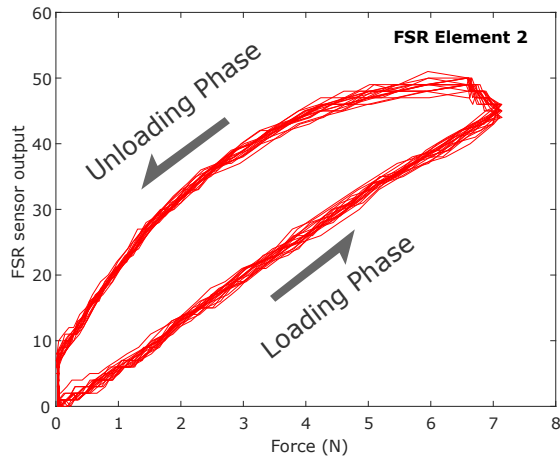
## VI. SOFTWARE DESIGN

### A. Sensor Characterization

For calibration purposes, we mount our sensor in series with a commercial force sensor, ATI Nano17 (ATI Industrial Automation, Apex, NC, USA), which provides the ground truth of the three-dimensional force vector applied to the sensor. These two sensors are mounted on the end-effector of a 6-DOF industrial robot. The robot is then controlled to probe a soft flat silicon slab at specific orientations while applying a specific force. In each measurement, the responses from our force sensor and ATI force sensor are recorded.



(a). Sensor response profile



(b). sensor element repeatability profile

Fig. 8: (a) Force response of the each element of the sensor vs the force measured using commercial sensor. (b) Repeatability profile of a sample FSR element over 20 cycles of loading and unloading.

In the first test, the robot was configured to probe the silicon slab perpendicularly with varying force. This test can be used to characterize the response, repeatability and hysteresis of the FSR material. The sensor outputs during 20

contact cycles for element 2 taken as an example are shown in Fig. 8(b), which demonstrated highly repeatable results with a hysteresis loop pattern. The relationship between normalized output of the four FSR elements and varying applied forces are shown in Fig. 8(a). The data were obtained by averaging the results from 20 repeated tests for each elements loading phases as shown in Fig. 8(b). Only data from loading phase were selected to calculate the sensor profile since they are more linear compared to those for unloading phase, due to characteristics of the sensor material itself. While the gradients of the responses from each element differ, they share the same property of being linear with the contact force. Thus this linearity of the sensor could be utilized to measure contact force.

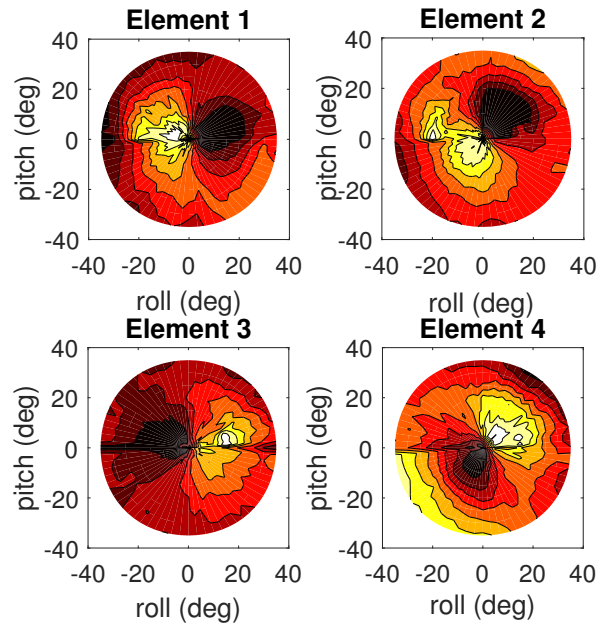


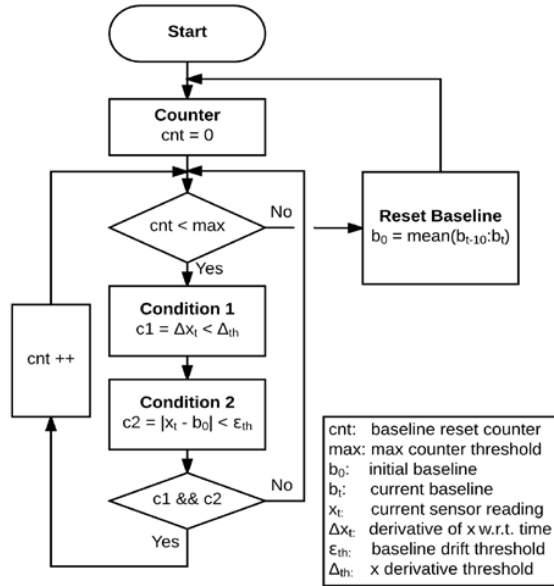
Fig. 9: A heat-map of each FSR array elements output, for varying contact force vector orientation.

In the second test, forces with the same amplitude and different orientations are applied. Each contour map in Fig. 9 shows the variation of the response of each element to the pitch and roll angles. The response has been normalized to compensate for the fluctuation in the magnitude of the force. For each element, the response is significantly high in a certain direction and low in the opposite direction. This information can be used to decode the direction of the force vector.

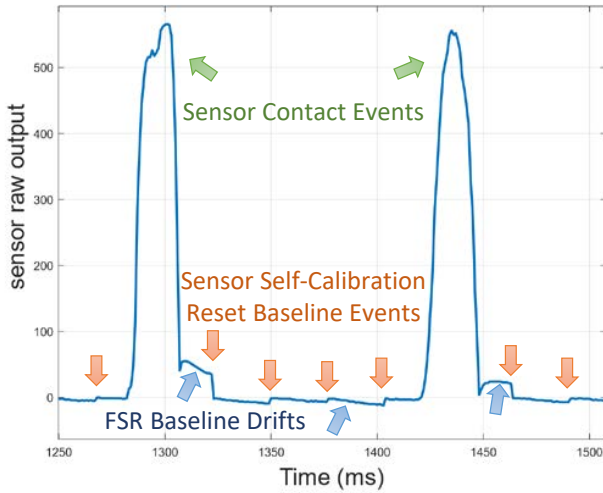
### B. Sensor Self-calibration Software

If the sensor is subjected to an external force, its zero-force output raw reading (referred to as baseline) changes due to the slight deformation of FSR material. To minimize this effect of an inconsistently shifting baseline on the accuracy of sensor reading, a baseline reset is implemented. The sensor self-calibration software flowchart is shown in Fig. 9(a), and the result of sensor self-calibration trials when the sensor is subjected to sporadic contact events is illustrated in Fig.

9(b). The threshold parameters tuning might be required to achieve optimal response for eliminating flow baseline drift while preserve sensitivity.



a). Sensor self-calibration software flowchart



b). Sensor raw output with self-calibration events plot

Fig. 10: (a) Self calibration software flow-chart and (b) sample results. The sensor is subjected to short (about 30ms) contacts (green arrows). The FSR baseline drifts (blue arrows) are shown to be corrected by the sensor self-calibration software at its reset baseline events (orange arrows).

## VII. EXPERIMENTS

### A. Stiffness Mapping

In open surgeries, physicians rely on sense of touch, vision and experience to identify hidden tumors, blood vessels and other stiff anatomical structures. However, typically in MIS, the sense of touch is lost and one needs to resort to using only visual information to discover abnormalities. While imaging

methods such as MRI and CT scan can provide preoperative information about the stiff elements in the anatomy, organ shift, swelling and other gravity induced deformation can cause a mismatch between preoperative data and the reality. Intraoperative ultrasound imaging has been developed to provide realtime information about the stiff inclusions [25], but the high cost of the tools have affected widespread acceptance. Recently, force sensing based solutions have

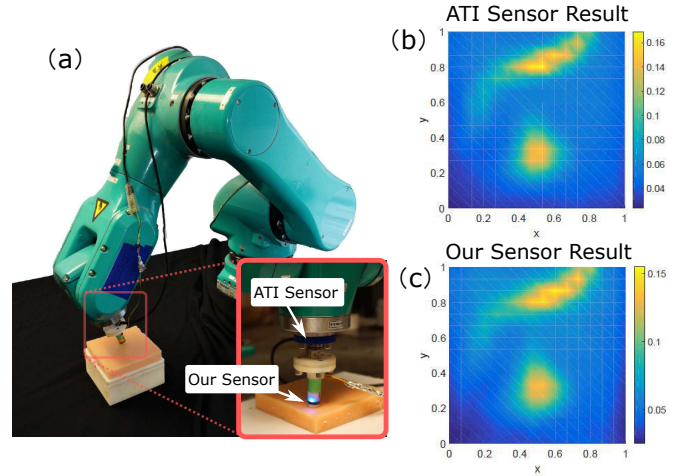


Fig. 11: Experimental setup and results for the stiffness mapping using a commercially available force sensor and our custom designed force sensor.

been proposed to detect the stiff inclusions [26], [27], [9], [28], [29], [30]. In this work, we mount our miniature force sensor at the tip of a 6-DOF robotic arm to estimate the stiffness distribution over the surface of a phantom silicon organ. As shown in Fig. 11(a) the silicon organ is placed in front of the robot arm and the robot is moved to a desired point on the surface of the organ. The robot is moved along the local surface normal up to a fixed depth of 1mm. The stiffness is computed as the magnitude of the force at the depth of 1mm. The organ is probed at several points arranged in a ‘raster-scan’ pattern. Fig. 11(b) shows the ground truth stiffness map as estimated by the commercial force sensor, ATI Nano17. Fig. 11(c) shows the stiffness map as estimated by our miniature force sensor. The stiffness map as estimated by our sensor conforms to the map generated by a commercial force sensor.

### B. Obstacle avoidance with a surgical snake robot

A highly articulated robotic probe (HARP) developed for deep intervention in MIS [2], [31] is used to demonstrate force-based obstacle detection and avoidance in this experiment. The HARP has six actuators, and is able to follow a specified curve in 3-dimensional space using a follow-the-leader mechanism [32]. In advancing mode, the first link of HARP moves forward while every other link advances along the trajectory of the snake. In steering mode, the first link can steer its orientation, while the rest of the links maintains their shape. An electro-magnetic (EM) sensor, trakSTAR™

(Ascension Technologies, Shelburne, VT, USA), is used to track the position and orientation of the first link of HARP, and provide feedback control during path-following.

The miniature force sensor is mounted at the tip of HARP. When the robot is commanded to autonomously follow a desired trajectory, the force sensor is able to detect any obstacles along the path, and provide feedback information to guide the robot to avoid obstacles. Fig. 12 shows the block diagram for control system architecture of the HARP. In steering mode, when an obstacle is detected by the force sensor, HARP is steered in the opposite direction according to the contact force vector directions. In advancing mode, if an obstacle is discovered, the robot stops advancing, retracts itself to the position before advancement, steers in the direction opposite to the obstacle, and then advances. In both situations, a virtual potential field is generated at the location where the obstacle is detected, to prevent HARP from running into the obstacle again. In this work, the

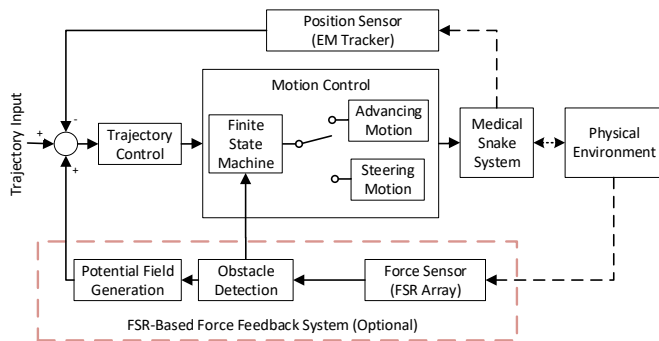


Fig. 12: Control block diagram for HARP.

experiment is conducted in a two-dimensional plane for the sake of simplicity. A circular block is used to simulate an unexpected obstacle on the predefined trajectory, while a bolt is used to represent the target to reach in the mission, as shown in Fig. 13. In the first demonstration, the force sensor is not in use and HARP is unaware of the obstacle on the way. As a result, it runs into the obstacle, pushes on the obstacle, and is not able to reach the goal location (see Fig. 13 (a)). In the second demonstration, on the contrary, the robot detects the obstacle on its way. Real-time feedback from the force sensor prevents HARP from disturbing the obstacle away and ensures that the contact force is small enough. The robot halts as soon as it makes contact with the goal object.

The demonstrations above show the benefits of using our force sensor with HARP. While the HARP has been telemanipulated so far for cardiac interventions [33], head and neck oncology [34] amongst others, the lack of force feedback has restricted autonomous navigation. We believe that the feedback from the miniature force sensor, coupled with optical fiber-based imaging at the tip of the robot would be the first step towards autonomous navigation of the HARP. Based on preoperative model of the anatomy, one can plan a nominal path for the robot, which can be constantly updated

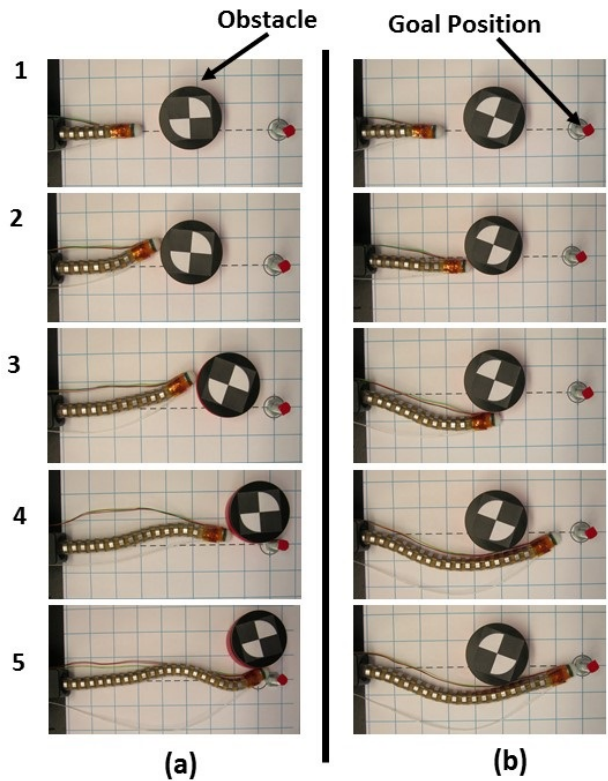


Fig. 13: Video screen shots of the HARP (a) failing to avoid the obstacle and disturbing the target without force sensing, and (b) successfully avoiding randomly placed obstacle and reaching the target using our force sensor.

in an online manner using the imaging and force feedback.

## VIII. CONCLUSION AND FUTURE WORK

This work introduces a novel miniature force sensor that is inexpensive, yet sensitive enough to be used in minimally invasive surgeries (MIS). The mechanical and electrical hardware design provides a reliable and accurate method for acquiring contact force vector. Through experiments on palpation-based stiffness mapping and force-based obstacle avoidance, we observe that the performance of the sensor is comparable to expensive off-the-shelf multi-axis force sensor. The signal processing firmware and force control software enables the possibility of integrating miniature tactile sensing into surgical robotic platforms. In addition to this, the design of the sensor makes it feasible to be fabricated at a low-cost both by small research labs or mass produced using standard PCB manufacturing services. Thus, our inexpensive force sensor can serve as a reference for generic tactile sensing applications limited by space constraints and cost, such as MIS, robotic manipulator and biologically inspired robots.

However, there is scope for improvement in the design that we plan to address in our future work. First, the preload force generation mechanism needs to be improved for greater reliability and repeatability over extended periods of use. For example, one option could be to use a custom designed

fastener as the fulcrum for the sensing array. Second, exploring other types of force sensing materials that provide better linearity with smaller baseline drifting. Third, sensing moments can be achieved by increasing the sensing array density or creating a 3D array structure. Lastly, creating a family of similar types of force sensing with different form factors for various applications. This includes asymmetrical or hollowed sensing array patterns, to allow better integration to existing MIS tools and surgical robots.

#### ACKNOWLEDGMENT

This work was supported by the National Robotics Initiative by NSF grant IIS-1426655. Special thanks to Florence Carton, Ben Brown, James Picard, Michael Schwerin and other colleagues from Biorobotics Lab, Carnegie Mellon University.

#### REFERENCES

- [1] A. Darzi and Y. Munz, "The impact of minimally invasive surgical techniques," *Annu. Rev. Med.*, vol. 55, pp. 223–237, 2004.
- [2] A. Degani, H. Choset, A. Wolf, and M. A. Zenati, "Highly articulated robotic probe for minimally invasive surgery," in *Proceedings of the IEEE International Conference on Robotics and Automation*. IEEE, 2006, pp. 4167–4172.
- [3] K. Xu, R. E. Goldman, J. Ding, P. K. Allen, D. L. Fowler, and N. Simaan, "System design of an insertable robotic effector platform for single port access (spa) surgery," in *IEEE/RSJ International Conference on Intelligent Robots and Systems*. IEEE, 2009, pp. 5546–5552.
- [4] B. Demi, T. Ortmaier, and U. Seibold, "The touch and feel in minimally invasive surgery," in *Haptic Audio Visual Environments and their Applications, 2005. IEEE International Workshop on*. IEEE, 2005, pp. 6–pp.
- [5] J. A. Flórez and A. Velásquez, "Calibration of force sensing resistors (FSR) for static and dynamic applications," in *Proceedings of the IEEE ANDESCON Conference*, 2010.
- [6] P. Puangmali, K. Althoefer, L. D. Seneviratne, D. Murphy, and P. Dasgupta, "State-of-the-art in force and tactile sensing for minimally invasive surgery," *IEEE Sensors Journal*, vol. 8, no. 4, pp. 371–381, 2008.
- [7] A. Trejos, R. Patel, and M. Naish, "Force sensing and its application in minimally invasive surgery and therapy: a survey," *Proceedings of the Institution of Mechanical Engineers, Part C: Journal of Mechanical Engineering Science*, vol. 224, no. 7, pp. 1435–1454, 2010.
- [8] T. Haidegger, B. Benyó, L. Kovács, and Z. Benyó, "Force sensing and force control for surgical robots," *IFAC Proceedings Volumes*, vol. 42, no. 12, pp. 401–406, 2009.
- [9] S. McKinley, A. Garg, S. Sen, R. Kapadia, A. Murali, K. Nichols, S. Lim, S. Patil, P. Abbeel, A. M. Okamura *et al.*, "A single-use haptic palpation probe for locating subcutaneous blood vessels in robot-assisted minimally invasive surgery," in *Automation Science and Engineering (CASE), 2015 IEEE International Conference on*. IEEE, 2015, pp. 1151–1158.
- [10] P. Baki, G. Székely, and G. Kósa, "Miniature tri-axial force sensor for feedback in minimally invasive surgery," in *4th IEEE RAS & EMBS International Conference on Biomedical Robotics and Biomechanics*. IEEE, 2012, pp. 805–810.
- [11] K. Xu and N. Simaan, "An investigation of the intrinsic force sensing capabilities of continuum robots," *IEEE Transactions on Robotics*, vol. 24, no. 3, pp. 576–587, 2008.
- [12] M. I. Tiwana, S. J. Redmond, and N. H. Lovell, "A review of tactile sensing technologies with applications in biomedical engineering," *Sensors and Actuators A: physical*, vol. 179, pp. 17–31, 2012.
- [13] B. L. Gray and R. S. Fearing, "A surface micromachined microtactile sensor array," in *Proceedings of the IEEE International Conference on Robotics and Automation*, vol. 1. IEEE, 1996, pp. 1–6.
- [14] U. Kim, D.-H. Lee, W. J. Yoon, B. Hannaford, and H. R. Choi, "Force sensor integrated surgical forceps for minimally invasive robotic surgery," *IEEE Transactions on Robotics*, vol. 31, no. 5, pp. 1214–1224, 2015.
- [15] J. Rausch and R. Werthschuetzky, "A miniaturised piezoresistive multi-component force sensor for minimally invasive surgery," *Proceedings of SENSOR 2009*, vol. 1, pp. 83–88, 2009.
- [16] J. Dargahi, M. Parameswaran, and S. Payandeh, "A micromachined piezoelectric tactile sensor for an endoscopic grasper-theory, fabrication and experiments," *Journal of Microelectromechanical Systems*, vol. 9, no. 3, pp. 329–335, 2000.
- [17] T. Hemsell, R. Stroop, D. O. Uribe, and J. Wallaschek, "Resonant vibrating sensors for tactile tissue differentiation," *Journal of Sound and Vibration*, vol. 308, no. 3, pp. 441–446, 2007.
- [18] S. I. Yaniger, "Force sensing resistors: A review of the technology," in *Electro International, 1991*, April 1991, pp. 666–668.
- [19] R. D. Klafater, T. A. Chmielewski, and M. Negin, "Robotic engineering: an integrated approach," *Prentice Hall*, p. 608, 1989.
- [20] K. Tadano and K. Kawashima, "Development of 4-DOFs forceps with force sensing using pneumatic servo system," in *Proceedings of the IEEE International Conference on Robotics and Automation*. IEEE, 2006, pp. 2250–2255.
- [21] Adafruit, "Pressure-Sensitive Conductive Sheet (Velostat/Linqstat)," 2017. [Online]. Available: <https://www.adafruit.com/product/1361>
- [22] H. Perner-wilson and M. Satomi, "Handcrafting Textile Sensors from Scratch."
- [23] S. LLC., "FSR 101 Force Sensing Resistor Theory and Applications," pp. 1–15, 2017.
- [24] K. Mustafa, "Filtering Techniques: Isolating Analog and Digital Power Supplies in TIs PLL-Based CDC Devices," *Texas Instrumentation (October 2001)*, 2001.
- [25] R. M. Comeau, A. F. Sadikot, A. Fenster, and T. M. Peters, "Intraoperative ultrasound for guidance and tissue shift correction in image-guided neurosurgery," *Medical physics*, vol. 27, no. 4, pp. 787–800, 2000.
- [26] R. A. Srivatsan, E. Ayvali, L. Wang, R. Roy, N. Simaan, and H. Choset, "Complementary model update: A method for simultaneous registration and stiffness mapping in flexible environments," in *IEEE International Conference on Robotics and Automation*. IEEE, 2016, pp. 924–930.
- [27] E. Ayvali, R. A. Srivatsan, L. Wang, R. Roy, N. Simaan, and H. Choset, "Using Bayesian Optimization to Guide Probing of a Flexible Environment for Simultaneous Registration and Stiffness Mapping," in *IEEE International Conference on Robotics and Automation*, 2016, pp. 931–936.
- [28] P. Puangmali, H. Liu, L. D. Seneviratne, P. Dasgupta, and K. Althoefer, "Miniature 3-axis distal force sensor for minimally invasive surgical palpation," *IEEE/ASME Transactions On Mechatronics*, vol. 17, no. 4, pp. 646–656, 2012.
- [29] P. Chalasani, L. Wang, R. Roy, N. Simaan, R. H. Taylor, and M. Kobilarov, "Concurrent nonparametric estimation of organ geometry and tissue stiffness using continuous adaptive palpation," in *IEEE International Conference on Robotics and Automation*. IEEE, 2016, pp. 4164–4171.
- [30] A. Garg, S. Sen, R. Kapadia, Y. Jen, S. McKinley, L. Miller, and K. Goldberg, "Tumor localization using automated palpation with gaussian process adaptive sampling," in *IEEE International Conference on Automation Science and Engineering*. IEEE, 2016, pp. 194–200.
- [31] R. A. Srivatsan, M. Travers, and H. Choset, "Using lie algebra for shape estimation of medical snake robots," in *Intelligent Robots and Systems*, 2014, pp. 3483–3488.
- [32] A. Degani, H. Choset, A. Wolf, T. Ota, and M. A. Zenati, "Percutaneous intrapericardial interventions using a highly articulated robotic probe," in *The first IEEE/RAS-EMBS International Conference on Biomedical Robotics and Biomechanics*. IEEE, 2006, pp. 7–12.
- [33] T. Ota, A. Degani, B. Zubiate, A. Wolf, H. Choset, D. Schwartzman, and M. A. Zenati, "Epicardial atrial ablation using a novel articulated robotic medical probe via a percutaneous subxiphoid approach," *Innovations (Philadelphia, Pa.)*, vol. 1, no. 6, p. 335, 2006.
- [34] C. M. Rivera-Serrano, P. Johnson, B. Zubiate, R. Kuenzler, H. Choset, M. Zenati, S. Tully, and U. Duvvuri, "A transoral highly flexible robot," *The Laryngoscope*, vol. 122, no. 5, pp. 1067–1071, 2012.